Journal of Alloys and Compounds 509 (2011) 1285–1293

Contents lists available at ScienceDirect

Journal of Alloys and Compounds

journal homepage: www.elsevier.com/locate/jallcom

Studies of nanostructured copper/hydrogenated amorphous carbon multilayer films

Neeraj Dwivedi[a], Sushil Kumar[a,*], Ishpal[a], Saurabh Dayal[a], Govind[b], C.M.S. Rauthan[a], O.S. Panwar[a]

[a] Plasma Processed Materials Group, National Physical Laboratory (CSIR), Dr. K.S. Krishnan Road, New Delhi 110012, India
[b] Surface Physics and Nano Structures Group, National Physical Laboratory (CSIR), Dr. K.S. Krishnan Road, New Delhi 110012, India

ARTICLE INFO

Article history:
Received 9 August 2010
Received in revised form
30 September 2010
Accepted 6 October 2010
Available online 14 October 2010

Keywords:
Multilayer
Low vacuum
Nanostructure

ABSTRACT

Nanostructured copper/hydrogenated amorphous carbon (a-C:H) multilayer grown in a low base vacuum (1×10^{-3} Torr) system combining plasma-enhanced chemical vapor deposition and sputtering techniques. These nanostructured multilayer were found to exhibit improved electrical, optical, surface and structural properties, compared to that of monolayer a-C:H films. The residual stresses of such multilayer structure were found well below 1 GPa. Scanning electron microscopy and atomic force microscopy results revealed a nanostructured surface morphology and low surface roughnesses values. X-ray photoelectron spectroscopy, secondary ion mass spectroscopy and energy dispersive X-ray analysis confirmed a very small amount of copper in these films. These structures exhibited very high optical transparency in the near infrared region (~90%) and the optical band gap varied from 1.35 to 1.7 eV. It was noticed that the temperature dependent conductivity improved due to the presence of both copper and the nano-structured morphology.

1. Introduction

Hard hydrogenated amorphous carbon (a-C:H), also called diamond like carbon (DLC), has evolved as one of the most versatile material in recent years. It contains tetrahedral diamond-like sp^3, trigonal graphite-like sp^2 and even sometimes linear sp^1 phases of carbon in its structure [1]. Because of both diamond and graphite like character, a-C:H exhibits unique electrical, optical, and tribological properties suitable for applications such as cutting tools, magnetic storage media and field emission devices [2–9]. Homo (a-C:H/a-C:H) and hetro (C–Si/a-C:H) junction solar cells and antireflection coatings on crystalline silicon solar cells are some of its recent applications realized [10–12]. It also finds application in the area of bio-implants due to its biocompatibility [13]. More recently, low temperature preparation of nanocrystalline diamond and carbon nanotube (CNT) embedded a-C:H thin films, prepared by plasma intensive technique, have attracted the attention of many researchers [14]. a-C:H, as a material has its limitation such as excessive residual stress and poor adhesion to the substrates which restrict its potential applications. However, these shortcomings may be reduced by the incorporation of foreign elements such as Si, N, F and various metals like Cu, Ti, etc. in the a-C:H matrix. Incorporation of such elements in a-C:H alters its properties by modifying the bonding structure. In addition, metal incorporation in a-C:H matrix not only reduces its residual stress but also improves adhesion, toughness and thermal stability of the film [15]. But the incorporation of nano-metallic particles in a-C:H matrix, using radio frequency (RF)-sputtering and radio frequency–plasma enhanced chemical vapor deposition (RF–PECVD) techniques is quite complex.

Voevodin et al. [16–18] have extensively studied various architectures of multilayer composite coatings with super hard a-C:H layers for wear protection at high contact loads. The use of a multilayer structure improves the adhesion of coatings to the substrates due to the inter layer present in the structures, which in turn minimizes the differences between the substrate and the coatings. By close examine, it is realized that metal/a-C:H multilayer has an additional advantage over other a-C:H structures that, in certain cases, metallic base layer, a few nanometers thick, in the multilayer structure of metal/a-C:H may also act as a catalyst for the formation of carbon nanostructures [19,20]. Multilayer structure of metal/a-C:H also find applications in the area of electronics and optics.

This paper reports the preparation and characterization of nanostructured copper/hydrogenated amorphous carbon (Cu/a-C:H) multilayer, grown using a hybrid system involving RF-sputtering and RF–PECVD techniques, at room temperature, and at a base pressure of 1×10^{-3} Torr. Four sets of multilayer structure were prepared with varying number of Cu/a-C:H bilayers, from one to four. After depositions, these structures were characterized for

* Corresponding author. Tel.: +91 11 45608650; fax: +91 11 45609310.
E-mail address: skumar@nplindia.org (S. Kumar).

0925-8388/$ – see front matter © 2010 Elsevier B.V. All rights reserved.
doi:10.1016/j.jallcom.2010.10.016

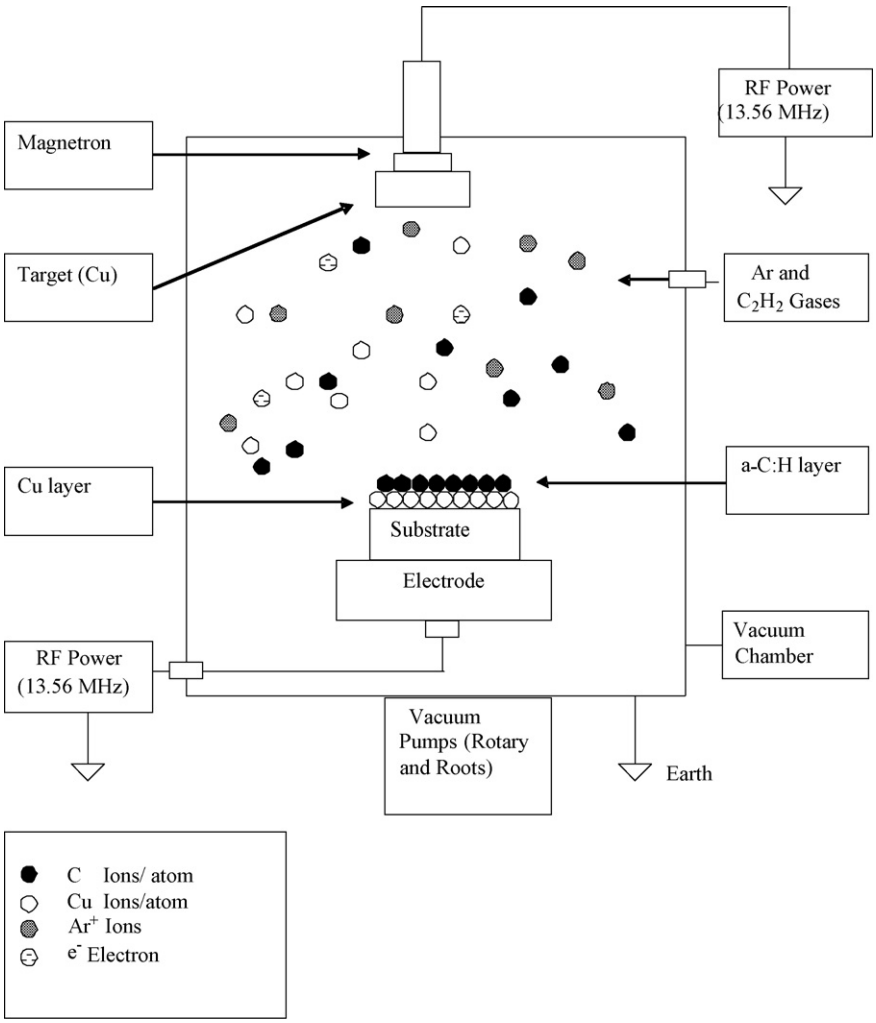

Fig. 1. Schematic representation of the deposition process in a hybrid system combining sputtering and PECVD techniques for the growth of Cu/a-C:H multilayer structure.

their surface, structural, transport, mechanical and optical properties.

2. Experimental details

Four Cu/a-C:H multilayer structure were deposited using a hybrid system involving RF-sputtering and RF–PECVD techniques, in the sequence of alternate layers of Cu and a-C:H, on well cleaned Si wafers, Corning 7059 glass, stainless steel sheet, and indium tin oxide coated glass substrates. Prior to the deposition of the multilayer structure, these substrates were also cleaned for 10 min in RF argon (Ar) plasma at a high negative self bias voltage of about 400 V. The ultimate base pressure for deposition was $\sim 1 \times 10^{-3}$ Torr in all the processes, which was achieved by a root blower pump backed by rotary pump. A Cu disk of 50 mm diameter was used as the metal sputtering target and the substrate to metal target distance was kept at about 6 cm. All depositions were carried out at constant negative self biases of 300 and 100 V for RF-sputtering and RF–PECVD processes, respectively, at constant Ar and acetylene (C_2H_2) gas pressures of 70 mTorr and 28 mTorr, respectively. Only the number of Cu/a-C:H bilayers (combination of one Cu and one a-C:H layer makes one Cu/a-C:H bilayer) were changed. The sample cdml-1, cdml-2, cdml-3 and cdml-4 contain one, two, three and four Cu/a-C:H bilayers, respectively, in the multilayer structure.

Fig. 1 is a schematic of the deposition unit used for the growth of Cu/a-C:H multilayer structure. Only single RF generator was used for growth of both Cu and a-C:H layers. During Cu layer deposition, the electrode on which the substrates were placed was connected to ground and RF power was applied to target electrode, while during a-C:H deposition, target electrode was connected to ground and RF power was applied to electrode on which substrates were placed. The parameters used for the deposition of Cu/a-C:H multilayer structure is summarized in Table 1.

The thickness of the sample cdml-1, cdml-2, cdml-3 and cdml-4 were found to be 56, 105, 154, 205 nm, respectively. The thickness of each Cu layer in the multilayer films was found to be ~15 nm. IBIS-Nanoindentation, Fisher–Cripps laboratories Pvt. Limited (Australlia), equipped with Berkovich indenter was used to measure the hardness and elastic modulus of multilayer coatings. The stresses in these multilayer films deposited on silicon wafer were determined from the change in the radius of curvature of the wafer, before and after deposition, using 500 TC temperature controlled film stress measurement system (M/s FSM Frontier Semiconductor, USA). The laser beam scans the surface of the wafer and the beam is deflected by the wafer surface which is detected by a position detector. If there is curvature induced in the wafer after deposition of film there will be change of position of the reflected beam. Curvature measurements were made by translating the sample a known distance X, along a direction perpendicular to the incident laser beam and measuring the displacement d of the reflected beam. Measurement of the reflected beam displacement was performed at a distance L from the sample. Using the values of X, d and L the radii of curvature R of a sample may be calculated by the relation:

$$R = \frac{2XL}{D}$$

The substrate curvature method generally relies on the Stoney formula relating the film average stress to the substrate curvature under the assumption that the film is much thinner than the underlying substrate. The Stoney formula, which was used to estimate residual stress is given in Eq. (1):

$$\sigma_f = \frac{E_s {d_s}^2}{6(1-\nu_s)d_f}\left(\frac{1}{R_f} - \frac{1}{R_0}\right) \quad (1)$$

where E_s, ν_s and d_s are Young's modulus, Poisson ratio and thickness of the substrate, respectively, and R_0 and R_f are the radii of substrate curvature before and after film deposition.

A scanning electron microscope (SEM Leo Electron Microscope model 7060) was used to study the microstructure of thin films. Energy dispersive X-ray (EDAX) was used to identify the presence of Cu and carbon in the deposited structures. Surface morphology, surface roughness, i.e. mean (Ra) and root mean square (RMS) roughnesses and particle size were analyzed using atomic force microscopy (AFM) instrument (model: nanoscope Veeco V). X-ray photoelectron spectroscopy (XPS) spectra of the films were obtained by Perkin Elmer 1257 instruments using X-

Table 1
Deposition parameters used for the growth of Cu/a-C:H multilayer structure.

Sample	Layer sequence	Ar pressure (mTorr), negative self bias (Volt)	C_2H_2 pressure (mTorr), negative self bias (Volt)	Thickness multilayer structure (nm)
cdml-1	Sub./Cu/a-C:H	70, 300	28, 100	56
cdml-2	Sub./Cu/a-C:H/Cu/a-C:H	70, 300	28, 100	105
cdml-3	Sub./Cu/a-C:H/Cu/a-C:H/Cu/a-C:H	70, 300	28, 100	154
cdml-4	Sub./Cu/a-C:H/Cu/a-C:H/Cu/a-C:H/Cu/a-C:H	70, 300	28, 100	205

ray radiation of Al Kα 1486.6 eV. Depth profile has been characterized by time of flight–secondary ion mass spectroscopy (TOF–SIMS), which is equipped with Bi-cluster ion analysis gun and sputter O_2 gun. Photoluminescence (PL) measurements were carried out at room temperature using Perkin Elmer LS 55 spectrometer. Transmission spectra were obtained by Shimadzu UV–VIS 1601 instrument. Dark conductivity measurements as a function of temperature was carried out from 298 to 473 K using a Keithley 610C Solid State electrometer on samples prepared in a coplanar structure, made by evaporating Al in a vacuum better than 10^{-5} Torr with a electrode separation of 0.078 cm.

3. Results and discussion

3.1. Hardness and elastic modulus

These Cu/a-C:H multilayer structure were characterized for their mechanical properties by nanoindentation and details are given elsewhere [21]. The values of hardness was found to decrease from 13 to 6 GPa with increase in number of Cu/a-C:H bilayers from one to four. Observed values of elastic modulus also followed similar trend and decreases from 177.3 to 100 GPa with the increase in number of Cu/a-C:H bilayers from one to four. It is to be noted that, observed moderate values of hardness and elastic modulus in Cu/a-C:H multilayer structures were due to following causes including (i) higher graphite-like sp^2 content, which is also confirmed by XPS analysis and (ii) high base pressure (1×10^{-3} Torr) growth of multilayer structure which involves several impurities. To elucidate more elastic properties in Cu/a-C:H multilayer structures, several other important mechanical parameters such as plastic resistance parameter (ratio between hardness and elastic modulus), elastic recovery (ER), ratio of residual displacement to displacement at maximum load (d_{res}/d_{max}) and plastic deformation energy (U_r) were also calculated [22]. The maximum value of plastic resistance parameter as 0.073 was observed in Cu/a-C:H multilayer structure containing one bilayer beyond which significant decrease in their values were observed that reveal more fraction of work is consumed in plastic deformation and large plastic strain is expected when contacting a material. In addition, the values of ER were also decreased from 57.6 to 47.4% with increase in number of Cu/a-C:H bilayers from one to four which revealed elastic–plastic behaviour of the deposited structures. Observed decrease of ER with increase in number of Cu/a-C:H bilayers was also satisfied by hardness values because hardness and ER vary proportional to each other. Similarly, observed elastic–plastic behaviour was also confirmed by d_{res}/d_{max} which was to be in the range between 0.42 and 0.52. Furthermore, observed decrease of U_r with increase in number of Cu/a-C:H bilayers one to four was also approved by hardness and ER results.

3.2. Residual stress

There are several studies reported in the literature that concern the methods to reduce the residual compressive stress in a-C:H films, either through incorporation of foreign elements in the a-C:H matrix [23,24] or by using a multilayer structure [25]. Delamination of the film from the substrate, due to high residual compressive stress, is one of the major issues with a-C:H films. In order to reduce the high residual compressive stress, four Cu/a-C:H multilayer structure were grown in which Cu and a-C:H layers were stacked on top of one another. The soft/hard layer concept is used here to minimize the residual stress in the multilayer structure. The thin soft Cu layers were grown using the RF-sputtering technique. This layer (interface layer) acts as an adhesive layer for the RF–PECVD grown hard a-C:H layer. It appears that one can obtain thick a-C:H films with a multilayer structure of Cu/a-C:H, because interfacial layers present in the multilayer structure reduce the residual compressive stress in the films as the soft/hard structure provides the needed relaxation in the overall structure. The pulsed plasma grown soft/hard DLC layer and Si containing DLC multilayer structure concept for the relaxation of the residual stress has been reported by Kumar et al. [26,27]. The soft Cu layer present in the multilayer structure acts as a metallic substrate for subsequent a-C:H layers and prevent the delamination of the multilayer structure. Fig. 2 shows the variation of residual compressive stress as a function of number of Cu/a-C:H bilayers in the multilayer structure. Initially, on increasing the Cu/a-C:H bilayers, the residual compressive stress of the structure was also increased but after a certain number of bilayers a small decrease in the stress was observed. The structure having one, two and three Cu/a-C:H bilayers exhibited residual compressive stress of the order of 0.5 GPa, 0.7 GPa and 0.85 GPa, respectively, which decreased to 0.75 GPa for the structure consisting of four Cu/a-C:H bilayers. It is worth noting that residual compressive stress present in all the multilayer structure studied was well below 1 GPa. Observed decrease of residual stress beyond three Cu/a-C:H bilayer structure may be due to the relaxation of the bonding at the interfaces. Thus, the multilayer having three Cu/a-C:H bilayers can be considered as threshold beyond which the relaxation in the residual stress was observed and below which there was increase in the residual stress with the increase of Cu/a-C:H bilayer from one to three.

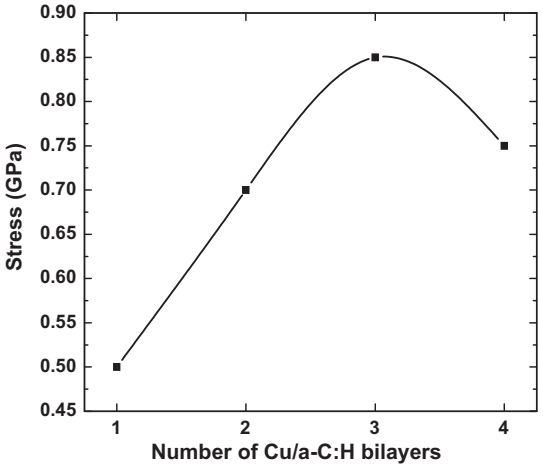

Fig. 2. Variation of residual stress versus number of Cu/a-C:H bilayers for multilayer structure.

3.3. SEM and AFM analysis

Fig. 3 shows the surface morphology of a Cu/a-C:H multilayer structure involving one, two, three and four bilayers (samples

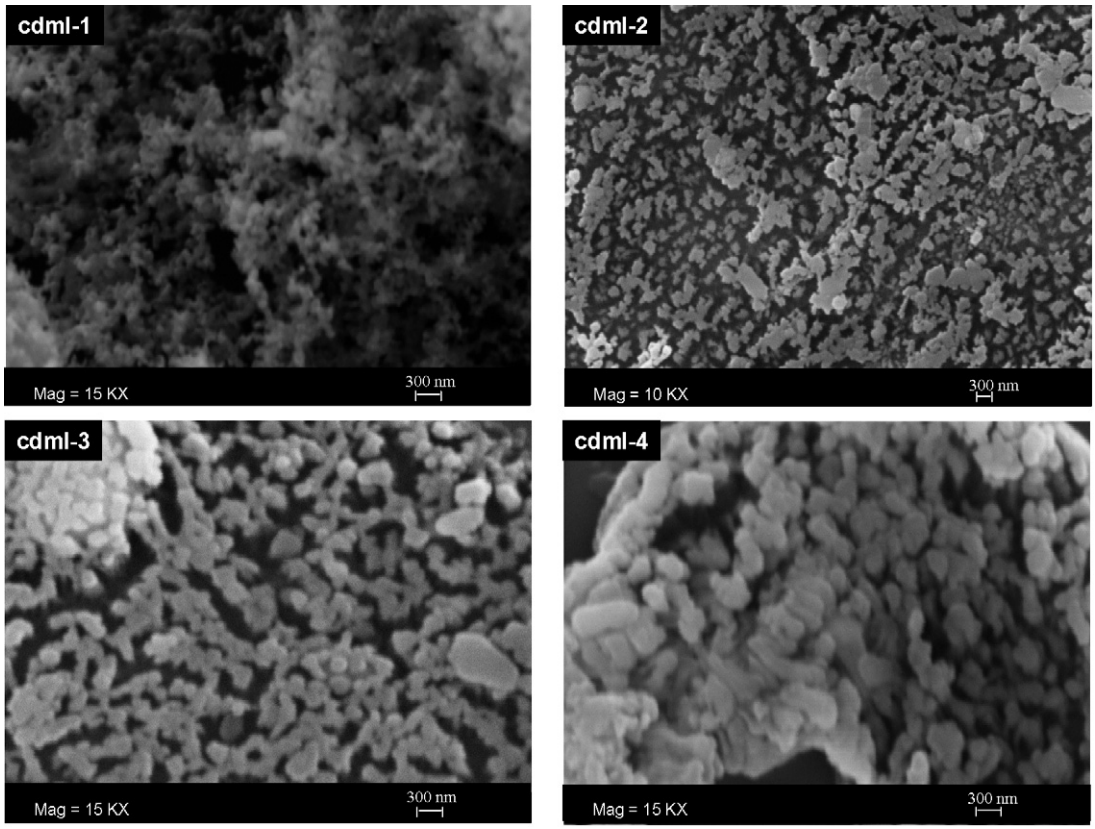

Fig. 3. SEM micrographs of Cu/a-C:H multilayer structure having one (cdml-1), two (cdml-2), three (cdml-3) and four (cdml-4) Cu/a-C:H bilayers.

cdml-1, cdml-2, cdml-3 & cdml-4), which reveal the formation of a nanostructured network on the surface of the multilayer structure. Since in all these multilayer structure, a-C:H layer was used as top layer therefore, it is expected that these may be carbon nano-agglomerates. It may also be possible that the metallic Cu layer acts as a catalyst for the growth of the said carbon nano-agglomerates. It is evident from these SEM micrographs that the size of these nano-agglomerates increase with increasing the number of Cu/a-C:H bilayers. The sample cdml-1 shows the presence of small nano-agglomerates which appear to be interconnected and form a long randomly oriented chain-like nanonetwork. With the increase in the number of Cu/a-C:H bilayers in the multilayer structure (for cdml-2), the sizes of these nano-agglomerates further increases. Observed chain-like network may help to improve the transport properties of the overall structures. However, a similar chain-like network is also observed for cdml-3 having three Cu/a-C:H bilayers. But the size of nano-agglomerates in this particular nanonetwork is larger. The SEM micrograph for cdml-4 containing four Cu/a-C:H bilayers in the structure exhibits the overlapping of these nano-agglomerates. It appears that the size of these nano-agglomerates has been further enhanced for this structure as compared to the previous structures. It is expected that, the metallic Cu layer present in the multilayer structure may play an important role in changing the structure of a-C:H from amorphous to nano-agglomerates, because nanotube and nanofiber like structure in thin film form have been studied previously, which had been obtained by growing a very thin metallic base layer prior to the amorphous carbon layer [20]. This kind of structure has also obtained by Ikuno et al. [28] and Bonard et al. [29]. Recently Mousinho et al. also reported the growth and characterization of nanocrystalline DLC films [30].

AFM has also been used to investigate the surface morphology, particle size and surface roughness of the Cu/a-C:H multilayer structure. A typical AFM image of a multilayer structure having four bilayers is shown in Fig. 4. It is evident from the AFM image that particles are uniformly distributed over entire surface of the structure and the surface is found to be very smooth. The values of average roughness (R_a), root mean square (RMS) roughnesses and particle size were found to be 0.73 nm, 0.92 nm and ~40–60 nm, respectively, for the multilayer structure having four Cu/a-C:H bilayers. The possible reason for this may be that the multilayer structure breaks the continuity of a single layer and thereby

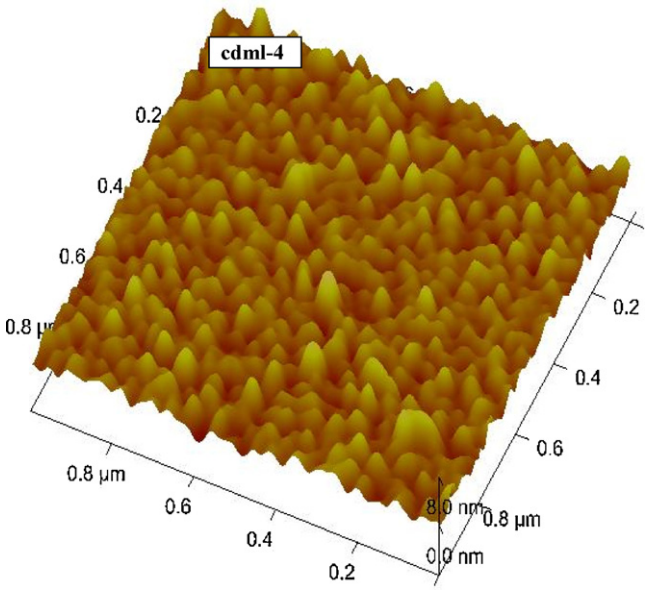

Fig. 4. Typical AFM picture of Cu/a-C:H multilayer structure having four (cdml-4) Cu/a-C:H bilayers.

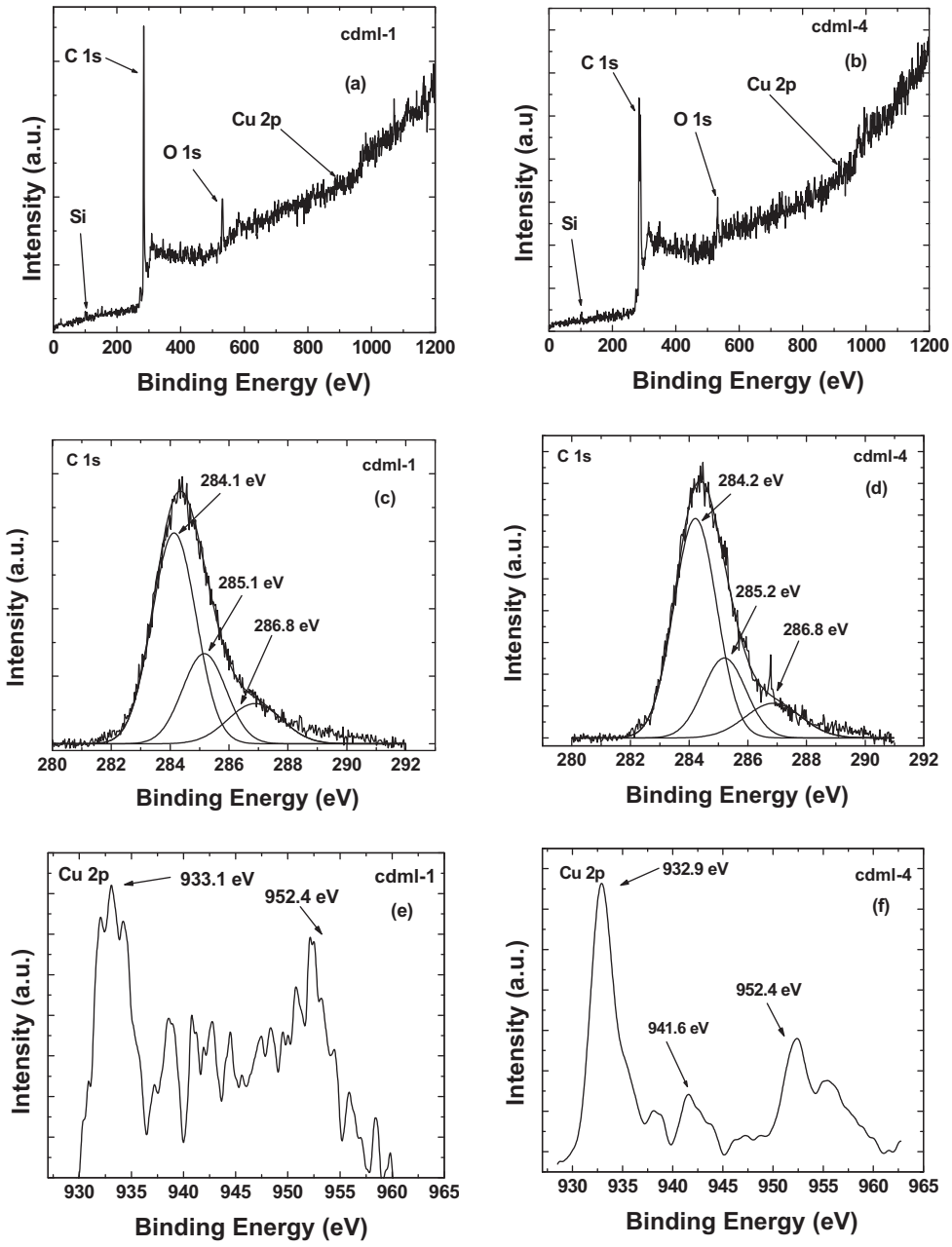

Fig. 5. XPS spectra of as grown Cu/a-C:H multilayer structure. (a) and (b) represent the general scan whereas (c) and (d) represent the deconvoluted core level spectra of C (1s). (e) and (f) represent the core level spectra of Cu.

reduces the defect generation. It is emphasized that as pure a-C:H is amorphous in nature whereas Cu/a-C:H multilayer exhibit nanostructured morphology. However, SEM images reveal that the RMS roughness value seems to be much larger than 0.92 nm. This could be due to images obtained by AFM and SEM was not from the same area of the sample. As AFM result was observed by probing one particular point whereas SEM result was obtained by scanning entire surface.

3.4. XPS analysis

XPS was used to investigate the chemical compositions, oxidation states and structural properties of the Cu/a-C:H multilayer structure. XPS spectra for as grown samples cdml-1 and cdml-4 are shown in Fig. 5(a)–(f). The general spectra as given in Fig. 5(a) and (b) for cdml-1 and cdml-4 revealed that oxygen is present with C 1s peak for these Cu/a-C:H multilayer structure. It is evident from the spectra that C and Cu peaks were found at their usual positions, but the intensity of the Cu peak in the general scan is found to be negligible. A similar observation has also been reported by Said et al. [31] for Ti doped DLC films. It is interesting to note that the Cu layer is covered under the nanostructured a-C:H layer. Therefore, core level spectra of Cu (2p) as shown in Fig. 5(e) and (f) in the binding energy range from 925 to 965 eV have been plotted to visualize the Cu peak. The presence of O (1s) peak in the spectra may be attributed to two facts: (i) deposition of these multilayer structure took place at comparatively high base pressure of the order of 1×10^{-3} Torr, which allowed some air dilution in the structures during its growth and (ii) prior to XPS measurements, the samples were exposed in ambient air which may led to surface contaminations. Jiang et al. [32] reported that oxygen plasma preferentially etches the soft graphitic like sp^2 C phase in the amorphous carbon

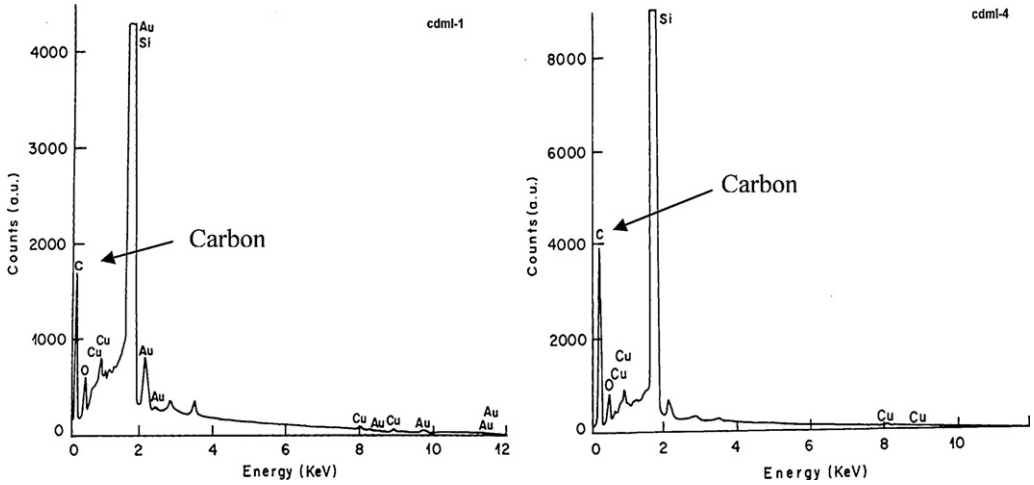

Fig. 6. EDAX spectrum of Cu/a-C:H multilayer structure containing one and four bilayers.

and carbon nitride films. Therefore, oxygen dilution may be useful for enhancing its mechanical properties.

Deconvoluted C 1s core level spectra for as deposited multilayer structure (cdml-1 and cdml-4) are shown in Fig. 5(c) and (d). The fitting of XPS C 1s core level spectra was performed by peak fit software using the Gaussian component. Since Cu does not form carbides (CuC), only three peaks in this particular core level spectrum have been fitted. These spectra exhibit two strong and one low intensity peak, which correspond to sp^3 C, sp^2 C and C–O bondings, respectively. Sample cdml-1 exhibited sp^3 C, sp^2 C and C–O peaks at the binding energy values 284.1, 285.1 and 286.8 eV, respectively, and changed to 284.2, 285.2 and 286.8 eV, respectively, for cdml-4 as shown in Fig. 5(c) and (d), respectively. The area under each component and the full width half maxima (FWHM) values, evaluated from various peaks present in the deconvoluted C 1s core level spectra are summarized in Table 2. The sp^2 C, sp^3 C and C–O bondings in cdml-1 contributed 60.4, 25.5 and 14.1% area, respectively, of the total area. However, in cdml-4 the area acquired by sp^2 C, sp^3 C and C–O bondings changed to 63.6, 23.2 and 13.2%, respectively. It is evident from the deconvoluted C 1s core level spectra that no significant changes in the values of area and FWHM were obtained for these two samples. Core level spectra of Cu (2p) are shown in Fig. 5(e) and (f), where two intense peaks are present in both the core level spectra centered at 933.1 and 952.4 eV for cdml-1, change to 932.9 and 952.4 eV for cdml-4. In cdml-4 (Fig. 5(f)), the satellite peak was observed at ~941.6 eV which was having 8.7 eV higher binding energy side from 932.9 eV. Similar difference (9 eV) in these two peaks has also been reported in literature [33,34]. The difference between the peaks of Cu $2P_{3/2}$ and Cu $2P_{1/2}$ is found to be about 19.5 eV. XPS data reveal that the binding energy position of Cu ($2P_{3/2}$) shifted to the higher binding energy in comparison to the pure Cu peak position (~932.6), which suggests that peak of Cu (2P) may have a contribution of CuO or Cu_2O. After analyzing the XPS result it is confirmed that this peak is of CuO because the binding energy of Cu_2O peak lies lower than pure Cu peak whereas the binding energy of CuO peak lies higher than pure Cu peak [33,35]. Similarly for cdml-1 the peak at 933.1 eV correspond to the CuO and the difference between the peaks of Cu $2P_{3/2}$ and Cu $2P_{1/2}$ is found to be about 19.3 eV.

3.5. EDAX analysis

EDAX measurement has also been performed to investigate the composition of the multilayer structure. Fig. 6 shows an EDAX spectrum of samples cdml-1 and cdml-4, which reveals the presence of strong C and lower intensity Cu peaks. In addition to C and Cu peaks, strong Si and O peaks in the spectra were observed and attributed to the fact that a Si substrate was used for the growth of the Cu/a-C:H multilayer structure. The reason for the presence of oxygen peak appears to be the high base pressure used in the growth of these structures (as evidenced by XPS results). Gold (Au) peak is also obtained in the spectra, since substrates were Au sputtered to make contact during SEM and EDAX measurements. The reason for using EDAX measurement along with XPS is that EDAX used high energy X-ray (from 0 to 10 keV) than XPS (which used X-ray photoelectron of few eV) for detecting the element composition of the deposited material. Therefore, from EDAX the material present even in the depth can also be identified. In the present case Cu always covered with a-C:H. Thus, by using EDAX it could be possible to find out Cu in the multilayer structure.

3.6. SIMS analysis

Due to some discrepancy occurred during analysis of XPS regarding presence of Cu, the depth profile of Cu/a-C:H multilayer structure was analyzed by secondary ion mass spectroscopy (SIMS). Fig. 7 shows the TOF–SIMS depth profiles for Cu, C, O and Si from Cu/a-C:H multilayer having four bilayers. The solid, dash, dot and bold solid lines represent the elements namely, C, Cu, O and Si, respectively. TOF–SIMS analysis gives a clear elemental demarcation between Cu and DLC layers. Figure clearly revealed the 4 steps

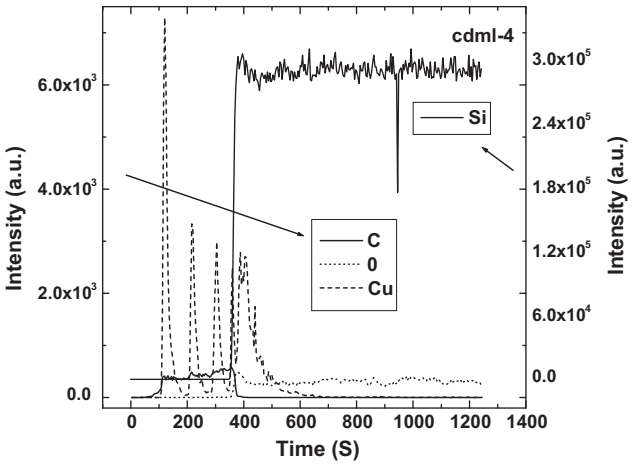

Fig. 7. Depth profile of Cu/a-C:H multilayer structure having four Cu/a-C:H bilayers.

Table 2
Peak position, area and FWHM values of deconvoluted C 1s core level spectra of cdml-1 (one Cu/a-C:H bilayer) and cdml-4 (four Cu/a-C:H bilayer).

Sample	Peak position (eV)	Bonding state	Area under the curve (%)	FWHM (eV)
cdml-1 (one bilayer)	284.1	sp^2 C	60.4	1.76
	285.1	sp^3 C	25.5	1.74
	286.8	C–O	14.1	2.16
cdml-4 (four bilayers)	284.2	sp^2 C	63.6	1.71
	285.2	sp^3 C	23.2	1.71
	286.8	C–O	13.2	2.24

of Cu within the certain intervals, which evident the existence of 4 Cu layer in the structures. It can be seen that, in comparison to that of Cu, no steps were observed for C. This may be due to (i) TOF–SIMS technique is very sensitive for metals like Cu and (ii) the hydrocarbon plasma always dominant in deposition system therefore, even during the growth of Cu layer, some carbon atoms travel in processing chamber and may be condensed over the growing structures. The TOF–SIMS depth profile also revealed the presence of significant amount of O in depth of this structure because of their high base pressure (1×10^{-3} Torr) depositions. At this high base pressure, sufficient air is diluted in the multilayer structures. However, very high intensity Si peak has been accounted to the fact that Si substrate was used for the growth of these Cu/a-C:H multilayer structure.

3.7. Photoluminescence (PL)

PL spectra of as deposited Cu/a-C:H multilayer structure having one and four Cu/a-C:H bilayers in its composition is shown in Fig. 8. A broad peak comprising of several small peaks was obtained in the visible range from 400 to 500 nm. The main PL peak for the structure having one Cu/a-C:H bilayer was centered at 447.5 nm which changed to 451.5 nm for the structure having four Cu/a-C:H bilayers.

It is observed that pure a-C:H film exhibits a PL peak centered near 600 nm [36]. However, in the Cu/a-C:H multilayer structure PL peaks were found at ~447.5 and ~451.5 nm for one and four bilayers, respectively. It is expected that carbon nano-agglomerates embedded in the a-C:H matrix may play a very vital role in the shifting of PL peaks from a higher wavelength region to a lower wavelength region (blue shift). The mechanism of PL in a-C:H can be explained on the basis that a-C:H contains both sp^2 and sp^3 sites.

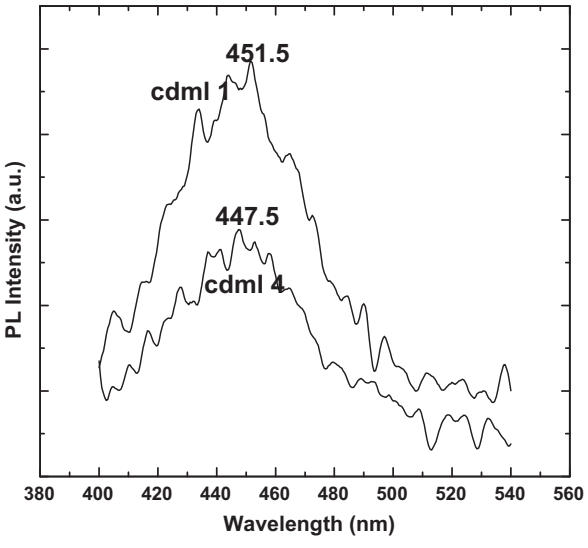

Fig. 8. Photoluminescence spectra of as deposited Cu/a-C:H multilayer structure having one and four Cu/a-C:H bilayers.

The sp^2 sites possess π states so their local band gap is much smaller than that of sp^3 sites which give rise to very strong fluctuations of the band edges. The strong fluctuations inhibit the mobility of carriers and provide a natural means to localize the electron–hole pair and result into efficient PL spectra [37]. PL in a-C:H can also be explained by cluster model. The electron–hole pairs are excited and recombine within clusters of sp^2 sites embedded in a sp^3-bonded matrix [37]. This localized transition within sp^2 cluster (from π to π^*) can be considered as band-to-band transition.

Particle size estimation for these multilayer structures was also done by PL spectra using Eq. (2) or (3) [38]:

$$E_i = E_g + \frac{h^2 \times \pi^2}{4\pi^2 \times 2\, m_r R^2} \tag{2}$$

or

$$R = \frac{h^2}{(8\, m_r\, E_i - E_g)^{1/2}} \tag{3}$$

where R is the particle size, m_r is the rest mass where $m_r = 0.125\ m_o$, E_i is the PL emission peak energy and E_g is the band gap of the material. However, the particle size estimated by this technique is found to be very low. The multilayer structure having one Cu/a-C:H bilayer shows a particle size about 1.45 nm, which changes to 1.63 nm for the structure having four Cu/a-C:H bilayers. It seems that there is a great difference in particle size for the multilayer structure as estimated by two different techniques, namely AFM and PL. It is not clear, why different values of particle size are obtained, but this may be due to the limitation of the AFM technique used in the present investigation to determine ultra nanoparticles present in the structures, whereas in PL even ultra nanoparticles may contribute to PL emission. The limitation of AFM technique may be due to artifact due to tip with the cantilever, if the radius of tip is relatively larger compared to the morphology of uneven film surface, the artifact affects to AFM images. There could also be possibility of the presence of smaller nanoparticles embedded in bigger nanoparticles, which cannot be observed in AFM image.

3.8. Transmission and optical band gap

Fig. 9 shows the transmission spectra of the multilayer structure of Cu/a-C:H, having one, two and three layers, in the range 325–1000 nm. The spectra reveal the high transparency (~90–95%) in the near IR region, inspite of the presence of metallic Cu layer in the multilayer structure. Further, the transmission and reflection measurements have been used to estimate the E_g values. The variation of E_g with the number of Cu/a-C:H bilayers is shown in the inset of Fig. 9. The values of E_g for these structures were estimated from plot $(\alpha h\nu)^{1/2}$ versus $h\nu$ curve by taking the asymptotic/ tangent of curve to the X axis. The values of E_g for these multi-structures varied between 1.35 and 1.7 eV. The structures having one, two and three Cu/a-C:H bilayers have E_g of 1.35, 1.47 and 1.7 eV, respectively, but a slight decrease in E_g was found, with a value of 1.6 eV for the structure having four Cu/a-C:H bilayers.

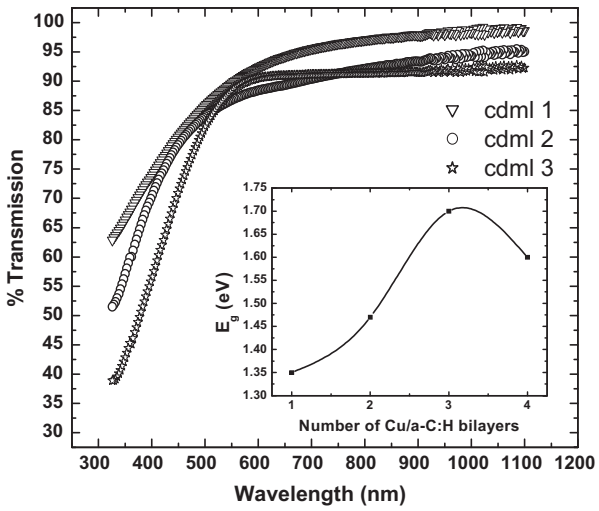

Fig. 9. Transmission spectra of Cu/a-C:H multilayer structure containing one, two and three Cu/a-C:H bilayers. The figure in inset shows the optical band gap variation of these multilayer structure as a function of the number of Cu/a-C:H bilayers.

3.9. Dark conductivity (σ_D)

Dark conductivity (σ_D) measurements on the Cu/a-C:H multilayer structure were performed on coplanar structures. a-C:H is a thermally conductive material in which conduction of charge carriers depends on trigonal graphite like sp^2 phase, associated with π to π^* weak bonds, because it contain one free electron in its structure. Generally a-C:H is considered to be insulating and its conductivity lies in the range of 10^{-12} to $10^{-8}\ \Omega^{-1}\ cm^{-1}$, but in the present investigation the conductivity in the multilayer structure varied from 10^{-9} to $10^{-4}\ \Omega^{-1}\ cm^{-1}$ in the temperature range 298–473 K. It is expected that metallic Cu layers in the structure play a very important role to enhance the value of σ_D. As SEM micrographs confirm the nanostructured network in the multilayer structure, these structures may also be responsible for enhancing the values of σ_D. It is evident from Fig. 10 that the multilayer structure having small nano-agglomeration (confirmed by SEM and AFM) exhibited higher value of σ_D and vice versa. On increasing the number of Cu/a-C:H bilayers in the multilayer structure, the number of interface layers (interface states) of the structure is also increased, which may lead to decrease in conductivity values. The variation of temperature dependent conductivity, (if the conduction is by a thermally activated process) is given by Eq. (4):

$$\sigma_D = \sigma_{01} \exp\left(\frac{-\Delta E_1}{kT}\right) + \sigma_{02} \exp\left(\frac{-\Delta E_2}{kT}\right) \quad (4)$$

where σ_D is the dark conductivity and σ_{01} and σ_{02} are conductivity pre exponential factors, ΔE_1 and ΔE_2 are two activation energies, k and T are the Boltzmann constant and the temperature, respectively.

Fig. 10 shows that each of these structures has a transition temperature at around 333 K, beyond which the slope of the variation of conductivity with inverse temperature changes. One process is dominant at higher temperatures and another process is dominant at lower temperatures. Below 333 K, the activation energy ΔE_2 appears to be dominant, and beyond 333 K, the activation energy ΔE_1 is dominant. The activation energy ΔE_2 for multilayer structure having one, two, three and four Cu/a-C:H bilayers was found to be 0.55, 0.27, 0.37 and 0.36 eV, respectively. However, values of activation energy ΔE_1 were found to be comparatively higher 0.77, 0.74, 0.71 and 0.75 eV, respectively.

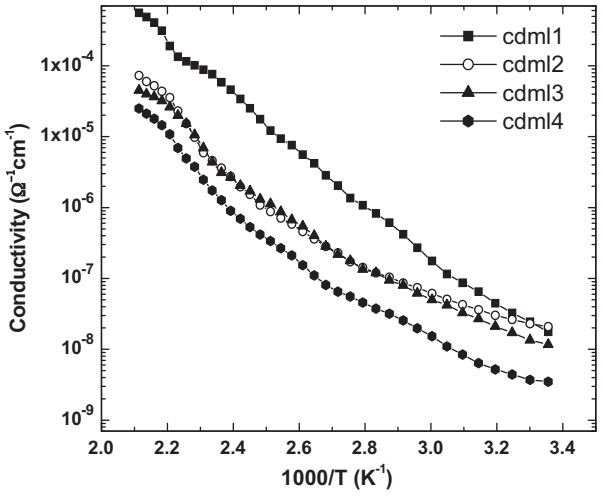

Fig. 10. Variation of σ_D versus inverse of temperature for as grown multilayer structure containing one, two, three and four Cu/a-C:H bilayers.

4. Conclusions

A hybridized system, involving RF–PECVD and RF-Sputtering techniques, operated at relatively high base pressure of 1×10^{-3} Torr was used to grow novel nanostructured Cu/a-C:H multilayer with the number of Cu/a-C:H bilayers varying from one to four. These structures exhibited multiple properties. The residual compressive stress of the multilayer structure was reduced considerably below 1 GPa. SEM and AFM micrographs revealed nanostructured networks and low roughness values. XPS, SIMS and EDAX spectra's confirmed the presence of Cu in the structure. By the estimation of sp^3 and sp^2 fraction of carbon from C 1s peak the multilayer structure were found to be of more graphite-like. The multilayer structure showed visible PL spectra, which were used to estimate the particle size. In spite of the presence of Cu in the multilayer structure, the optical transparency of these structures in the visible and near IR region was not significantly affected. The values of E_g were found to be in the range of 1.35 to 1.7 eV for various Cu/a-C:H multilayer structure. Temperature dependent transport improved due to the presence of nanostructured network.

In conclusion, observed decrease in stress and improvement in electrical and optical properties by employing Cu/a-C:H multilayer structure grown at low base vacuum condition in a low cost system could be useful for cost effective coatings not only for protecting soft surfaces such as hard coating on cutting tools, hard and protective coating on solar cells, wear resistance coating on magnetic storage media; but may also for electronic, optical and optoelectronic applications.

Acknowledgements

The authors are grateful to the Director, National Physical Laboratory, New Delhi (India) for his kind support. Authors wish to thank Dr. B.R. Chakraborty, Mr. Samantha, Mr.- K.N Sood, Mr. Sandeep and Mr. Jai for providing SIMS, AFM and SEM characterization facilities, respectively. Authors are grateful to MNRE government of India for providing NRE fellowship to Mr. Neeraj Dwivedi. This research is sponsored by CSIR, Govt. of India, through the Network Project NWP-0027.

References

[1] J. Robertson, Semicond. Sci. Technol. 18 (2003) S12.
[2] T. Itoh, N. Mutsukura, Vacuum 77 (2004) 11.

[3] S. Singh, M. Pandey, R. Kishore, N. Chand, S. Dash, A. Tyagi, Plasma Process. Polym. 5 (2008) 853.
[4] C. Godet, S. Kumar, V. Chu, Philos. Magz. 83 (2003) 3351.
[5] S.S. Tinchev, Y. Dyulgerska, P. Nikolova, D. Grambole, U. Kreissing, T. Babeva, J. Optoelect. Adv. Mater. 8 (2006) 308.
[6] A. Grill, IBM Res. Dev. 43 (1999) 147.
[7] O.S. Panwar, S. Kumar, S.S. Rajput, R. Sharma, R. Bhattacharya, Vacuum 72 (2004) 183.
[8] H.S. Zhang, J.L. Endrino, A. Anders, Appl. Surf. Sci. 255 (2008) 2551.
[9] H.-S. Zhang, K. Komvopoulos, J. Appl. Phys. 105 (2009) 83305.
[10] K.M. Krishna, M. Umeno, Y. Nukaya, T. Soga, T. Jimbo, Appl. Phys. Lett. 77 (2000) 1472.
[11] B. Gupta, A. Kapoor, R.M. Mehra, T. Soga, T. Jimbo, M. Umeno, Sol. Energy Mater. Sol. C 79 (2003) 305.
[12] V.G. Litovchenko, N.I. Klyui, Sol. Energy Mater. Sol. C 68 (2001) 55.
[13] A. Bruinink, A. Schroeder, G. Francz, R. Hauert, Biomaterials 26 (2005) 3487.
[14] R.C. Smith, J.D. Carey, C.H.P. Poa, D.C. Cox, S.R.P. Silva, J. Appl. Phys. 95 (2004) 3153.
[15] S. Zhang, D. Sun, Y. Fu, H. Du, Surf. Coat. Technol. 198 (2005) 2.
[16] B.C. Yeldose, B. Ramamoorthy, Int. J. Adv. Manuf. Technol. 38 (2008) 705.
[17] A.A. Voevodin, S.D. Walck, J.S. Zabinski, Wear 203–204 (1997) 516.
[18] A.A. Voevodin, J.S. Zabinski, C. Muratore, Tsinghua Sci. Technol. 10 (2005) 665.
[19] Z. Zhang, P. He, Z. Sun, T. Feng, Y. Chen, H. Li, B.K. Tav, Appl. Surf. Sci. 256 (2010) 4417.
[20] A. Malesevic, S. Vizireanu, R. Kemps, A. Vanhulsel, C.V. Haesendonck, G. Dinescu, Carbon 45 (2007) 2932.
[21] N. Dwivedi, S. Kumar, D. Kaur, C.M.S. Rauthan, O.S. Panwar, Optoelect. Adv. Mater.: Rapid Commun. 4 (2010) 604.
[22] N. Dwivedi, S. Kumar, C.M.S. Rauthan, O.S. Panwar, Appl. Phys. A, (2010), doi:10.1007/s00339-010-5908-5.
[23] Y. Pauleau, F. Theiry, P.B. Barna, F. Misjak, A. Kovacs, S.N. Dub, V.V. Uglov, A.K. Kuleshov, Rev. Adv. Mater. Sci. 6 (2004) 140.
[24] M.J. Dai, K.S. Zhou, S.S. Lin, H.J. Hou, X.G. Zhu, H.W. Li, S.C. Niu, Plasma Process. Polym. 4 (2007) S215.
[25] M. Gioti, S. Logothetidis, C. Charitidis, Appl. Phys. Lett. 73 (1998) 184.
[26] S. Kumar, P.N. Dixit, D. Sarangi, R. Bhattacharyya, J. Appl. Phys. 85 (1999) 3866.
[27] S. Kumar, N. Goyal, P.N. Dixit, C.M.S. Rauthan, Proc of the 51st SVC Annual Technical Conference, Chicago, 2008, p. 722.
[28] T. Ikuno, T. Yamamoto, M. Kamizono, S. Takahashi, H. Furuta, S.I. Honda, S. Ohkura, M. Katayama, T. Hirao, K. Oura, Phys. B 323 (2002) 171.
[29] J.M. Bonard, M. Croci, C. Klinke, R. Kurt, O. Noury, N. Weiss, Carbon 40 (2002) 1715.
[30] A.P. Mousinho, R.D. Mansano, M.C. Salvadori, J. Alloys Compd. 495 (2010) 620.
[31] R. Said, N. Ali, C.A.A. Ghumman, O.M.N.D. Teodoro, W. Ahmed, J. Nano Sci. Nanotechnol. 8 (2008) 1.
[32] L. Jiang, A.G. Fitzgerald, M.J. Rose, R. Cheung, B. Rong, E.V. Drift, Appl. Surf. Sci. 193 (2002) 144.
[33] J. Ghijsen, L.S. Tjeng, J.V. Elp, H. Eskes, Phys. Rev. B 38 (1988) 11322.
[34] C.D. Wagner, W.M. Riggs, L.E. Davis, J.F. Moulder, G.E. Muilenberg, Handbook of X-ray Photoelectron Spectroscopy, Perkin Elmer Corporation, 1979.
[35] S. Paulston, P.M. Parlett, P. Stone, M. Bowker, Surf. Interf. Anal. 24 (1996) 811.
[36] M. Pandey, D.S. Patil, Diamond Relat. Mater. 16 (2007) 1912.
[37] Rusli, G.A.J. Amaratunga, J. Robertson, Phys. Rev. B 53 (1996) 16306.
[38] E. Edelberg, S. Bergh, R. Naone, M. Hall, E.S. Aydil, J. Appl. Phys. 81 (1997) 2410.